Strain mapping with parts-per-million resolution in synthetic type-Ib diamond plates

Albert T. Macrander,[a] Szczesny Krasnicki, Yuncheng Zhong, Josef Maj, and Yong S. Chu
Advanced Photon Source, Argonne National Laboratory, 9700 South Cass Avenue, Argonne, Illinois 60439-4800

(Received 27 July 2005; accepted 27 September 2005; published online 3 November 2005)

A general method to map strain with parts per million (ppm) resolution in single-crystal wafers and plates is demonstrated. An x-ray technique has been used to obtain separate maps of strain and tilt across synthetic diamond growth sectors. Data consisting of rocking curve maps obtained with a charge coupled device detector were analyzed. The strain results image the growth sectors and reveal a strain pileup near the sector boundaries. The diamond was yellow to the eye due to nitrogen impurities. Not only the topography of the strain map, but also the strain magnitudes, are consistent with the strain arising from nitrogen impurities. High strain resolution in the ppm range is needed to observe these effects. © *2005 American Institute of Physics*. [DOI: 10.1063/1.2126790]

Strain from point defects in large single crystals has a deleterious effect for many applications. It is generally undesirable for x-ray optics for synchrotron beamlines because of the attendant broadening of the rocking curve.[1] Another example of deleterious affects of strain is the degradation in the performance of electronic and optoelectronic devices built on single-crystal wafers having a large inherent mismatch between an epitaxial layer and the substrate.[2]

X-ray methods for strain determination have been revolutionized by the availability of charge coupled device (CCD) cameras, and the consequent mapping of strain at a level of 10^{-4} or above has been reported by several groups.[3,4] Strain maps with much higher sensitivity can be obtained from shifts of x-ray rocking curves. In general, one must separate the effect of changes in the local orientation from that of local strain since orientation variation is a generally occurring and significant effect.[5] We report here on high-resolution mapping measurements of strain due to nitrogen impurities in diamond plates of type Ib that demonstrate the power of the method.

Nitrogen is an impurity in type-Ib synthetic diamonds grown by the high-pressure-high-temperature process[6] and causes an increase in the lattice parameter.[5] The relationship between the diamond lattice expansion and the concentration of N, c_N, is given by Ref. 5 $\Delta a/a=0.14c_N$, where a is the lattice parameter. During the crystal growth process, different crystallographic facets develop at different rates to produce a faceted stone. The facets can be grouped into growth sectors having equivalent Miller indices, and in the order of increasing tendency to contain N, these are: {110}, {113}, {100}, and {111}.[5,6] The {110} sector has been reported to have very low N uptake and has been used as a reference for quotation of strain by Lang *et al.*[5] When a stone is sawed into slabs, an outline of the boundaries at which two sectors abutted during the crystal growth is evident in x-ray topographic images.[7]

Strain and tilt can be separately obtained.[8] The technique relies on pairs of measurements of rocking curves made at 180° azimuthal rotation around the reciprocal lattice vector for the x-ray diffraction. Shifts in the position of the rocking curves are due to the combined effect of tilt and strain, and from the two rocking curve measurements, they can be determined separately. The technique has been applied previously to diamond, but only at selected sample locations.[5,7,9] The technique has not been applied to obtain detailed maps of strain and tilt. Other workers have made rocking curve mapping analyses but only for the lattice tilt variation (diamond[10] and GaAs[11]). A brief conference report of some preliminary results has previously appeared.[12] A related technique to map out strain in InP due to dislocations was presented at the same conference.[13] There are several possible sources of error in the alignment and in goniometer movements, and the data analyses must be done so that the proper pixels in two separate images are paired.

The measurements were made in a double-crystal alignment with a rotating anode x-ray source, where the first crystal was a Si monochromator and the second crystal was the diamond sample set for the (004) reflection. An asymmetrically cut Si(531) monochromator was applied to expand the Cu $K\alpha$ x-ray beam dimension to 70 mm.[14] The angle between the incident x-ray beam and the monochromator surface was 0.7°. The rotating anode was operated at 60 kV and 300 mA. The sample was mounted on a stage capable of an azimuthal rotation. The angular stability of the monochromator and the sample was at least 0.1 arcsec. The crystal was a synthetic diamond procured from Drukker (recently renamed as Element Six).

The system incorporated two easily interchangeable detectors. A scintillation detector was used for sample alignment. A CCD camera (resolution $60\times 60\ \mu\text{m}^2$) was used to obtain mapping data by recording a rocking curve for each pixel. After alignment, rocking curves were recorded with an angular step of 0.5 arcsec. Data collection time per exposure was 20 s. Data collection times for two azimuthal pairs were less than 3 h, and the temperature changes at the sample were $\leqslant 0.5$ °C over this time period.

The measured rocking curve shift can be generally expressed as the sum of two terms,[8]

[a]Author to whom correspondence should be addressed; electronic mail: macrander@aps.anl.gov

0003-6951/2005/87(19)/194113/3/$22.50 © 2005 American Institute of Physics
Downloaded 04 Nov 2005 to 164.54.53.70. Redistribution subject to AIP license or copyright, see http://apl.aip.org/apl/copyright.jsp

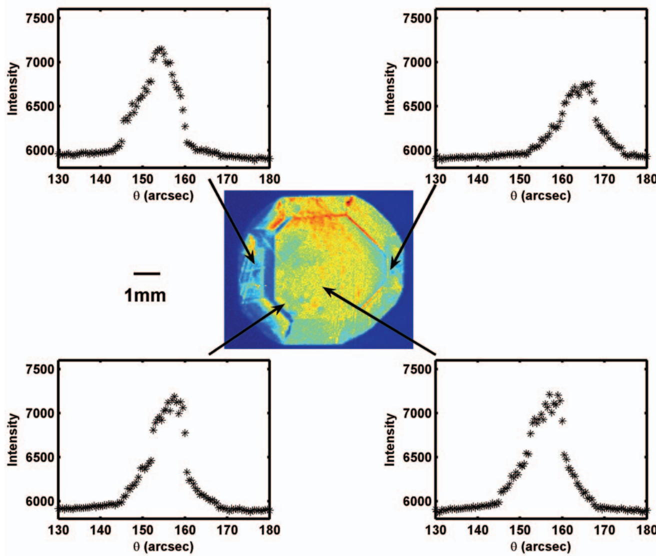

FIG. 1. (Color) An x-ray topograph obtained at the peak of the overall average rocking curve and representative rocking curves for isolated pixels. A CCD baseline offset has not been subtracted.

$$\Delta\theta = (\tan\,\theta_B)\Delta d/d + (\hat{n}_r \cdot \hat{n}_m)\Delta\varphi, \qquad (1)$$

where $\Delta\theta$ is the rocking curve shift relative to a reference position, d is the lattice spacing, Δd is the lattice spacing variation, θ_B is the Bragg angle, $\Delta\varphi$ is the misorientation angle, $\hat{n}_r$ and $\hat{n}_m$ are the directions of the rocking curve rotation axis and the misorientation rotation axis, respectively. For convenience, the reference position was taken as the position of the average rocking curve of the whole sample, that is the average over all pixels. The lattice spacing and the misorientation information can be separated by obtaining rocking curves at azimuthal rotations that are 180° apart[5,8] since then the sign of misorientation term in Eq. (1) changes but the strain term is not altered. It follows that

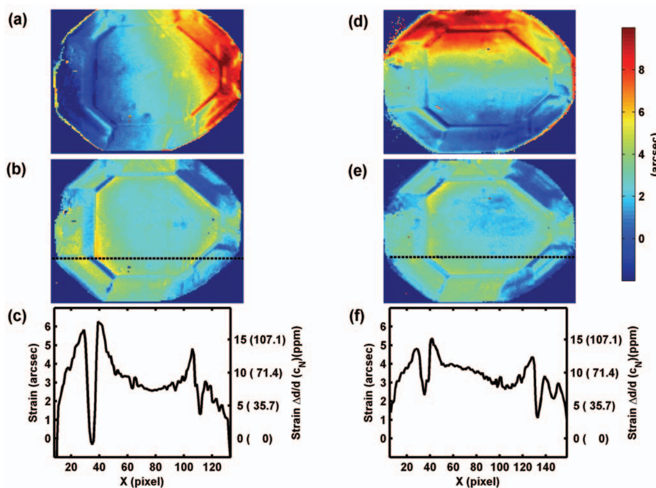

FIG. 2. (Color) The separated maps of tilt, (a) $\Delta\varphi_x$ and (d) $\Delta\varphi_y$, and strain $(\Delta d/d)$ (b) and (e). The separated tilt/strain contributions to the rocking curve shifts are shown in a color scale calibrated in arc seconds as shown. Here, (a) and (b) are from 0°/180° pair, and (d) and (e) are from the 90°/270° pair. A cross cut of the strain profile at the dotted lines is shown in (c) corresponding to strain map in (b), and in (f) corresponding to the strain map in (e). The right side ordinate scales in (c) and (f) is converted to $\Delta d/d$ as well as to the corresponding concentration of nitrogen. The difference between (c) and (f) is indicative of the precision achieved. The standard deviation of the differences in $\Delta d/d$ is 1.6 ppm.

$$\Delta d/d = (\mathrm{ctg}\ \theta_B)[\Delta\theta(0°) + \Delta\theta(180°)]/2,$$

$$\Delta\varphi_x = [\Delta\theta(0°) - \Delta\theta(180°)]/2,$$

$$\Delta\varphi_y = [\Delta\theta(90°) - \Delta\theta(270°)]/2, \qquad (2)$$

where $\Delta\theta(\rho)$ is the shift measured at azimuthal angle ρ, and $\Delta\varphi_{x,y}$ are the misorientation angles about two arbitrary but perpendicular rotation axes lying roughly in the sample surface.

Systematic errors stem from slight misalignments between the diffraction vector and the axis of azimuthal rotation. In addition, the diffraction planes of the sample and of the monochromator must be closely parallel. We have found reproducible results if these misalignments are all less than 0.1°.

For pixel-by-pixel analysis, it is important to locate the same point on the sample from the images taken at different azimuthal angles. The Cartesian coordinates of one point at different azimuthal angles can be traced through a pair of linear transformation which accounts for rotation, scaling, and translation of the original points. The six required transformation parameters can be determined from three pairs of known coordinates, which we have labeled as characteristic points. The characteristic points are taken at easily distinguishable points, such as a corner.

The basis of the foregoing pixel-by-pixel analysis lies in the one-to-one spatial correspondence between the image and the diamond plate, that is, the diffracted x rays reaching one pixel should be from a counterpart region on the sample. This condition is well satisfied if the angular spread caused by lattice tilts and by strain is smaller than the angular acceptance of one pixel, which is the present case. The detector pixel size of our system is 60 μm, and the distance from the crystal to the detector is 30 cm, which corresponds to an angular acceptance of 41 arcsec for one pixel. This angular acceptance is much larger than the tilt angle and the contribution due to strain in the present case, indicating that the x rays reaching one pixel on a CCD are almost entirely diffracted from the same small region on the sample. We note that the spatial resolution of the maps is altered by the choice of the pixel size, but the precision of the strain determination is not affected by this choice. This follows because the angle through which the sample is rocked is recorded and not the

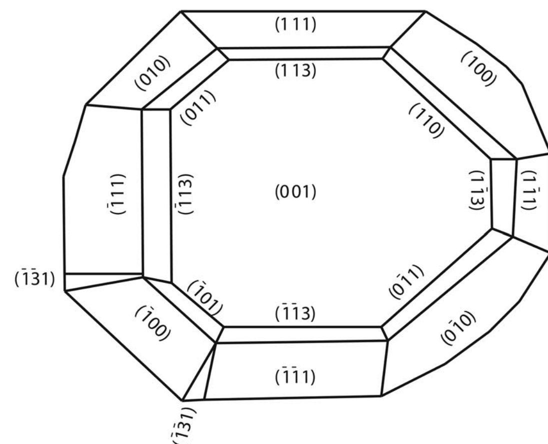

FIG. 3. Growth sector indexing assignments.

Downloaded 04 Nov 2005 to 164.54.53.70. Redistribution subject to AIP license or copyright, see http://apl.aip.org/apl/copyright.jsp

scattering angle (often denoted as 2θ), with each pixel acting as a detector over a range of x-ray scattering angles.

Representative rocking curves are shown in Fig. 1 along with a x-ray topograph obtained at the peak of the overall average rocking curve. In general, the rocking curves showed asymmetries characteristic of a depth-dependent strain and/or tilt. Rocking curve positions were assigned according to the center point at half maximum intensity. We have studied the depth dependence in this diamond,[15] and we found that despite the depth dependence, most of the diffracted intensity arises from within an extinction depth of the surface, 12.6 μm. That the depth dependence of the strain and lattice tilts does not perturb rocking curve shifts sufficiently to negate the present analysis is an implicit assumption, and a significant aspect of the present work is a test of this assumption. We find good agreement with literature reports for growth-sector features despite the possible depth dependence, consequently, we infer that the depth dependence over the extinction depth is weak.

The separation into tilt and strain for two azimuthal pairs is shown in Fig. 2. Sector boundaries are evident in these maps. The growth sectors closely resemble x-ray topographs reported by Wierzchowksi *et al.*[7] for an (001)-oriented slab, and they have been indexed as shown in Fig. 3. We find agreement with the ordering of the sectors according to their N uptake as detailed above, and we have used the {110} sector as a null-strain reference. A new result presented here is the quantitative strain profile across the central {001} growth zone and the elevated strain near the sector boundaries. The resultant N concentration obtained via Eq. (1) is also indicated in Figs. 2(c) and 2(f) and has a maximum of 107 ppm, a value consistent with previous reports.[5,6,16]

The method itself affords a means to assess the net affect of possible errors. This can be done by comparing results for the two azimuthal pairs shown in Fig. 2. The distribution of differences in $\Delta d/d$ was obtained. A Gaussian was found to be a good fit to the distribution, and the attendant standard deviation for our strain determinations as obtained from this fit was 1.6 ppm.

In summary, we have demonstrated mapping of strain with ppm precision. A strain pileup near growth-sector boundaries in a synthetic diamond plate is reported for the first time. The mapping technique can be applied, in general, to single-crystal wafers and plates that have low inherent strain and a low mosaic spread.

Note added in proof. The tilt maps contain a contribution due to wavelength dispersion.

This work was supported by the U.S. Department of Energy, Basic Energy Sciences-Materials Science, under Contract No. W-31-109-ENG-38.

[1] D. Keith Bowen and Brian K. Tanner, *High Resolution Diffractometry and Topography* (Taylor Francis, London, 1998).
[2] V. Swaminathan and A. T. Macrander, *Materials Aspects of GaAs and InP Based Structures* (Prentice–Hall, New York, 1991).
[3] Y.-A. Soh, P. G. Evans, Z. Cai, B. Lai, C.-Y. Kim, G. Aeppli, N. D. Mathur, M. G. Blamire, and E. D. Isaacs, J. Appl. Phys. **91**, 7742 (2002).
[4] J. D. Budai, W. Yang, N. Tamura, J.-S. Chung, J. Z. Tischler, B. C. Larson, G. E. Ice, C. Park, and D. P. Norton, Nat. Mater. **2**, 487 (2003).
[5] A. R. Lang, M. Moore, A. P. W. Makepeace, W. Wierzchowski, and C. M. Welbourn, Philos. Trans. R. Soc. London **337**, 497 (1991).
[6] R. C. Burns, V. Cvetkovic, C. N. Dodge, D. J. F. Evans, M. T. Rooney, P. M. Spear, and C. M. Welbourn, J. Cryst. Growth **104**, 257 (1990).
[7] W. Wierzchowski, M. Moore, A. P. W. Makepeace, and A. Yacoot, J. Cryst. Growth **114**, 209 (1991).
[8] U. Bonse, Zh. Eksp. Teor. Fiz. **153**, 278 (1958).
[9] G. Kowalski, M. Moore, G. Gledhill, and Z. Maricic, J. Phys. D **29**, 793 (1996).
[10] J. Hoszowska, A. K. Freund, E. Boller, J. P. F. Sellschop, G. Level, J. Hartwig, R. C. Burns, M. Rebak, and J. Baruchel, J. Phys. D **34**, A47 (2001).
[11] P. Mikulik, D. Lubbert, D. Korytar, P. Pernot, and T. Baumbach, J. Phys. D **36**, A74 (2003).
[12] S. Krasnicki, Y. Zhong, J. Maj, and A. Macrander, Proc. SPIE **5195**, 40 (2003).
[13] C. Ferrari, N. Verdi, D. Lubbert, D. Korytar, P. Mikulik, T. Baumbach, L. Helfen, and P. Pernot, Proc. SPIE **5195**, 84 (2003).
[14] S. Krasnicki, Rev. Sci. Instrum. 67, Paper C28, CDROM only (1996).
[15] Y. Zhong, S. Krasnicki, A. T. Macrander, Y. S. Chu, and J. Maj, J. Phys. D **38**, A39 (2005).
[16] H. Sumiya, N. Toda, and S. Satoh, J. Cryst. Growth **237**, 1281 (2002).

Downloaded 04 Nov 2005 to 164.54.53.70. Redistribution subject to AIP license or copyright, see http://apl.aip.org/apl/copyright.jsp